ACS OMEGA

Article

Cite This: ACS Omega 2018, 3, 5202−5211

Heterometallic Octanuclear $Ni^{II}_4Ln^{III}_4$ (Ln = Y, Gd, Tb, Dy, Ho, Er) Complexes Containing $Ni^{II}_2Ln^{III}_2O_4$ Distorted Cubane Motifs: Synthesis, Structure, and Magnetic Properties

Pankaj Kalita,[†] Joydeb Goura,[†,§] Juan Manuel Herrera,[‡] Enrique Colacio,*[,‡] and Vadapalli Chandrasekhar*[,§,∥]

[†]School of Chemical Sciences, National Institute of Science Education and Research, Homi Bhabha National Institute, Jatni, Khurda, Bhubaneswar 752050, Odisha, India

[‡]Departamento de Química Inorgánica, Facultad de Ciencias, Universidad de Granada, Avenida de Fuentenueva s/n, 18071 Granada, Spain

[§]Department of Chemistry, Indian Institute of Technology Kanpur, Kanpur 208016, India

[∥]Centre for Interdisciplinary Sciences, Tata Institute of Fundamental Research Hyderabad, Gopanpally, Hyderabad 500107, India

Supporting Information

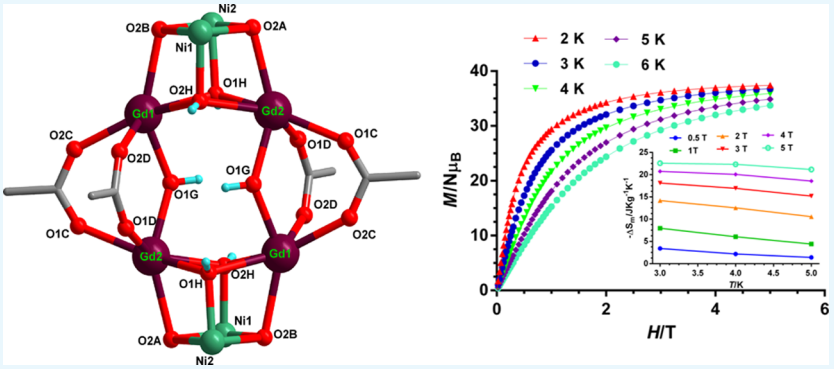

ABSTRACT: The reaction of 2-methoxy-6-[{2-(2-hydroxyethylamino)ethylimino}methyl] phenol (LH_3) with lanthanide metal salts followed by the addition of nickel acetate allowed isolation of a family of octanuclear complexes, $[Ni_4Ln_4(\mu_2\text{-}OH)_2(\mu_3\text{-}OH)_4(\mu\text{-}OOCCH_3)_8(LH_2)_4]\cdot(OH)_2\cdot xH_2O$. Single crystal X-ray diffraction studies of these complexes reveal that their central metallic core consists of two tetranuclear $[Ni_2Ln_2O_4]$ cubane subunits fused together by acetate and hydroxide bridges. The magnetic study of these complexes reveals a ferromagnetic interaction between the Ln^{III} and the Ni^{II} center. The magnitude of exchange coupling between the Ni^{II} and Ln^{III} center, parametrized from the magnetic data of the Gd analogue, gives J = +0.86 cm^{-1}. The magneto caloric effect, studied for the $Ni^{II}_4Gd^{III}_4$ complex, shows a maximum of magnetic entropy change, $-\Delta S_m$ = 22.58 J kg^{-1} K^{-1} at 3 K for an applied external field of 5 T.

INTRODUCTION

The discovery of single-molecule magnets (SMMs) is now nearly 2 decade old, yet this field continues to grow unabated with several contributions each year. The first example of a SMM is a Mn_{12} complex, and this spurred interest in polynuclear transition metal complexes.[1−5] The cumulative understanding as a result of studies on several such complexes leads to the understanding that in polynuclear transition metal complexes a high spin ground state (S) and a negative magnetic anisotropy (D) should be present to achieve high anisotropic energy barriers (U_{eff}) for magnetization reversal.[6−8] Although a large spin ground state can be achieved in exchange-coupled polynuclear transition metal complexes, the S and D parameters are found to be inversely proportional to each other and therefore there appears to be a limit to the extent of increasing U_{eff} by modulating S.[9−13] It was soon realized that the single-ion anisotropies, particularly of lanthanide ions might be gainfully harnessed for achieving interesting magnetic properties in molecular complexes.[14−18] One of the approaches to take advantage of the lanthanide anisotropy is to design molecular magnets containing heterometallic 3d/4f complexes.[19−24] We have been working in assembling and studying various types of 3d/4f complexes.[25−27] Among the numerous 3d/4f complexes reported in the literature, including from our laboratory, polynuclear Ni^{II}/Ln^{III} complexes are gaining interest because of the ferromagnetic exchange interaction that is often seen between the lanthanide and nickel center.[28−32] In view of this interest, we were interested in exploring new Ni^{II}/Ln^{III}

Received: February 19, 2018
Accepted: April 30, 2018
Published: May 14, 2018

DOI: 10.1021/acsomega.8b00292
ACS Omega 2018, 3, 5202−5211

Scheme 1. Synthesis of Ni_4Ln_4 Complexes

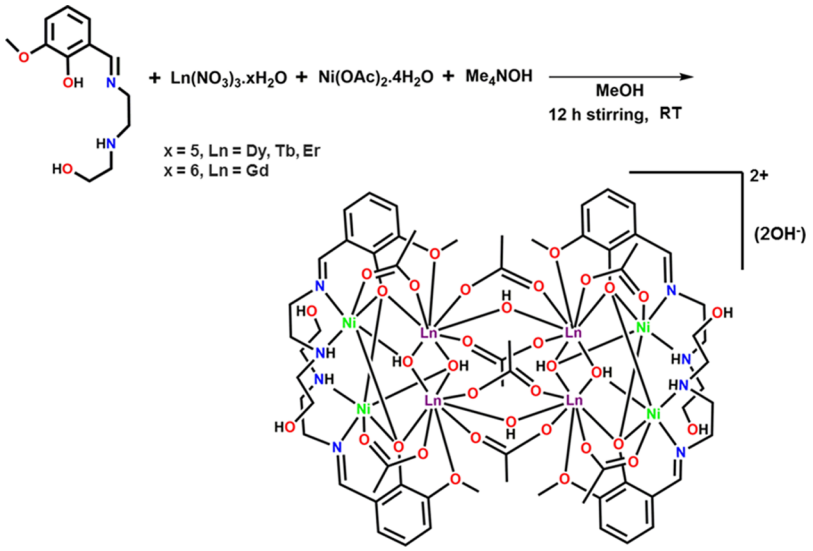

Table 1. Crystal Data and Refinement Parameters for Complexes 1−6

	1	2	3	4	5	6
chemical formula	$C_{64}H_{98}Y_4N_8Ni_4O_{34}\cdot 2(OH)$	$C_{64}H_{98}Gd_4N_8Ni_4O_{34}\cdot 2(OH)$	$C_{64}H_{98}Tb_4N_8Ni_4O_{34}\cdot 2(OH)$	$C_{64}H_{98}Dy_4N_8Ni_4O_{34}\cdot 2(OH)$	$C_{64}H_{98}Ho_4N_8Ni_4O_{34}\cdot 2(OH)$	$C_{64}H_{98}Er_4N_8Ni_4O_{34}\cdot 2(OH)$
M_r	2147.99	2421.35	2428.03	2442.35	2452.07	2461.39
crystal system, space group	monoclinic, $P2_1/n$	monoclinic, $P2_1/n$	monoclinic, $P2_1/n$	monoclinic, $P2_1/n$	monoclinic, $P2_1/n$	monoclinic, $P2_1/n$
temperature (K)	100(2)	100(2)	100(2)	100(2)	100(2)	100(2)
a, b, c (Å)	12.9768(12), 15.5079(15), 23.549(2)	12.8381(6), 15.4317(6), 23.4889(10)	12.9219(6), 15.516(1), 23.5346(13)	12.832(3), 15.413(3), 23.419(5)	12.9771(7), 15.5019(8), 23.5655(13)	12.9222(3), 15.4758(3), 23.46589(4)
β (deg)	96.737(1)	96.593(3)	96.576(3)	96.765(4)	96.714(3)	96.601(1)
V (Å^3)	4706.3(8)	4622.7(3)	4687.6(5)	4599.6(16)	4708.2(4)	4661.61(16)
Z	2	2	2	2	2	2
radiation type	Mo Kα	Mo Kα	Mo Kα	Mo Kα	Mo Kα	Mo Kα
μ (mm^{-1})	3.298	3.704	3.840	4.088	4.180	4.428
crystal size (mm)	0.17 × 0.15 × 0.11	0.15 × 0.12 × 0.10	0.16 × 0.13 × 0.11	0.14 × 0.11 × 0.08	0.14 × 0.12 × 0.09	0.15 × 0.13 × 0.10
reflections collected	32 167	70 774	71 751	24 420	34 917	86 231
GOOF on F^2	1.012	1.046	1.058	1.052	0.978	1.007
unique reflections [R_{int}]	10 018 [R_{int} = 0.0653]	11 503 [R_{int} = 0.0595]	11 609 [R_{int} = 0.0814]	8541 [R_{int} = 0.0633]	10 164 [R_{int} = 0.0545]	14 305 [R_{int} = 0.0833]
no. of parameters	531	540	504	536	539	536
no. of restraints	4	5	4	4	3	5
$\Delta\rho_{max}$, $\Delta\rho_{min}$ (e Å^{-3})	1.28, −0.94	1.92, −1.34	2.01, −1.37	1.70, −1.43	1.30, −1.06	1.65, −1.36
density (g cm^{-3})	1.516	1.740	1.720	1.763	1.730	1.753
completeness to θ	99.6% (26.799°)	99.5% (28.365°)	99.6% (28.295°)	99.6% (25.449°)	99.1% (26.978°)	99.7% (30.592°)
limiting indices	$-16 \le h \le 16$, $-17 \le k \le 19$, $-29 \le l \le 28$	$-17 \le h \le 17$, $-20 \le k \le 20$, $-31 \le l \le 31$	$-17 \le h \le 17$, $-20 \le k \le 14$, $-31 \le l \le 31$	$-14 \le h \le 15$, $-18 \le k \le 18$, $-28 \le l \le 21$	$-16 \le h \le 16$, $-19 \le k \le 16$, $-29 \le l \le 28$	$-18 \le h \le 18$, $-22 \le k \le 21$, $-33 \le l \le 33$
θ range (deg)	2.627−26.799	1.582−28.365	2.059−28.295	1.585−25.499	2.63−26.978	1.897−30.592
F(000)	2192.0	2392	2400	2408	2416	2424
final R indices [$I > 2\sigma(I)$]	R_1 = 0.0457, wR_2 = 0.0959	R_1 = 0.0349, wR_2 = 0.0833	R_1 = 0.0520, wR_2 = 0.1333	R_1 = 0.0472, wR_2 = 0.1115	R_1 = 0.0357, wR_2 = 0.0757	R_1 = 0.0430, wR_2 = 0.0977
R indices [all data]	R_1 = 0.0920, wR_2 = 0.1098	R_1 = 0.0439, wR_2 = 0.0866	R_1 = 0.0900, wR_2 = 0.1574	R_1 = 0.0694, wR_2 = 0.1300	R_1 = 0.0542, wR_2 = 0.0831	R_1 = 0.0844, wR_2 = 0.1159
CCDC no.	1586139	1581911	1581909	1581902	1581920	1581912

complexes. In an earlier study from our laboratory, we have used the 2-methoxy-6-[{2-(2-hydroxyethylamino)ethylimino}-methyl]phenol (LH_3) ligand to assemble the heterometallic Fe^{III}/Ln^{III} and $Co^{III}_2Ln^{III}$ complexes.[33−35] The latter was found to be an SMM even at zero applied magnetic field with the highest reversal of energy barrier so far reported in the

DOI: 10.1021/acsomega.8b00292
ACS Omega 2018, 3, 5202−5211

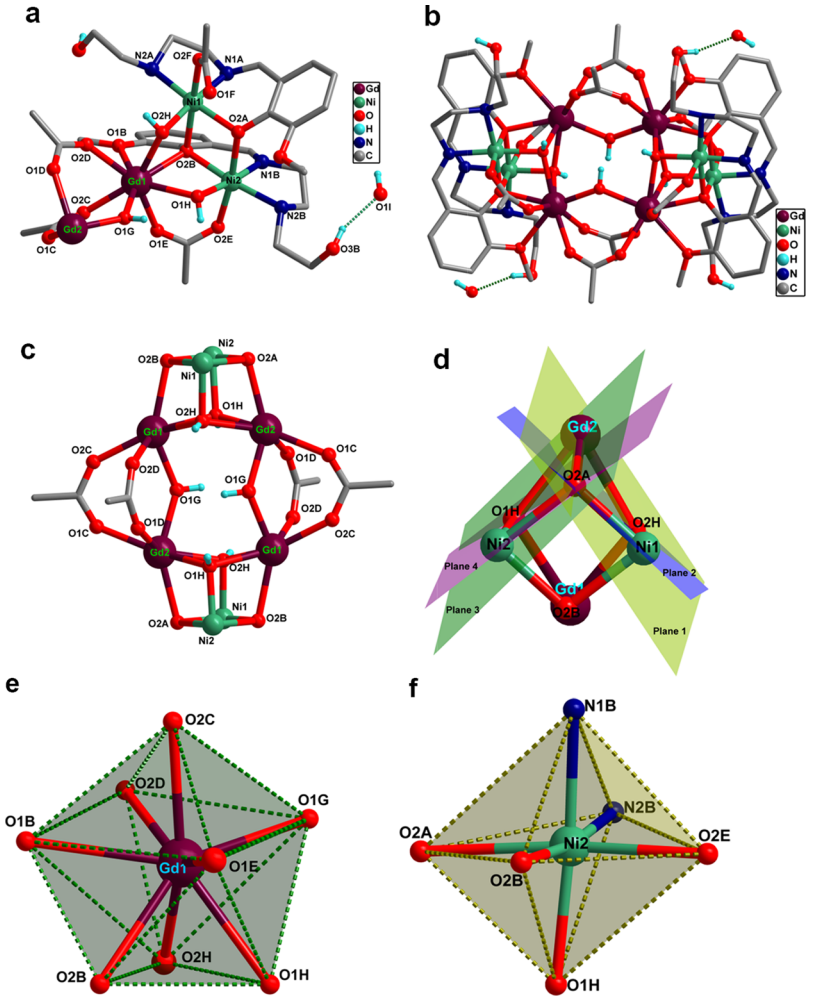

Figure 1. (a) Asymmetric unit of **2**. (b) Molecular structure of **2**. (c) Octanuclear core of **2**. (d) Dihedral angle between the O–Ni^{II}–O and O–Gd^{III}–O planes. (e) Coordination environment/geometry around Gd^{III} showing a distorted trigonal dodecahedron geometry. (f) Coordination environment/geometry of Ni^{II} showing a distorted octahedral geometry.

literature for such type of complexes.[34] It was of interest to us to study the coordination behavior of LH_3 toward the assembly of Ni^{II}/Ln^{III} complexes. Accordingly, herein, we report a series of Ni_4Ln_4 complexes (Ln = Y, (**1**); Gd, (**2**); Tb, (**3**); Dy, (**4**); Er, (**5**); Ho, (**6**)). These complexes are composed of two heterometallic $Ni^{II}_2Ln^{III}_2O_4$ distorted cubes connected to each other by acetate and hydroxide bridging ligands. The synthesis, characterization, and magnetism of these complexes are discussed herein.

RESULTS AND DISCUSSION

Synthetic Aspects. Polyfunctional compartmental ligands with O-donor and N-donor atoms are the most commonly used ligands for the construction of heterometallic 3d/4f complexes, many of which exhibit interesting magnetic properties.[36−39] Appropriate design of ligands with specific binding compartments that can selectively coordinate to lanthanide and transition metal ions allows the preparation of 3d/4f heterometallic compounds. We have been involved in the design of such ligands for some time and have successfully assembled many 3d/4f complexes. In this context, we have prepared a multipocket compartmental Schiff base ligand based on an ethylenediamine central motif flanked by two unsymmetrical O-donor functional units. Previously, we have used this ligand to prepare a Co_2Dy complex which revealed a zero-field SMM behavior.[34] In view of this, we were interested to explore if this ligand could be used for preparing other heterometallic 3d/4f complexes containing Ni^{II}. Accordingly, the ligand 2-methoxy-6-{[2-(2-hydroxyethylamino)ethylimino]methyl}-phenol (LH_3) was allowed to react with nickel acetate and lanthanide metal salts in the presence of tetramethyl ammonium hydroxide in a 1:1.1:2 stoichiometric ratio to afford dicationic octanuclear complexes, **1**−**6** (Scheme 1).

Molecular Structures. The molecular structures of the complexes **1**−**6** were confirmed by single crystal X-ray crystallography. The crystal data and refinement parameters for **1**−**6** are summarized in Table 1. All the complexes are isostructural and crystallized in the monoclinic crystal system with the $P2_1/n$ space group. The asymmetric unit of all these complexes contains one-half of the molecule (two monodeprotonated ligand $[LH_2]^-$, two lanthanide ions, two nickel ions, four bridging acetate ions, and three bridging hydroxylato ions) (see Figure 1a). This cationic asymmetric unit is charge-balanced by a hydroxide ion hydrogen-bonded with the ligand periphery.

The coordination modes of all the participating ligands in **1**−**6** are summarized in Supporting Information (see Figure S6). The nature of the bridging hydroxylato ligand present in all the

DOI: 10.1021/acsomega.8b00292
ACS Omega 2018, 3, 5202−5211

complexes has been confirmed by bond valence sum (BVS) calculations (see Table S1; Supporting Information). In view of the overall structural similarity of the complexes, the molecular structure of $[Ni_4Gd_4(\mu_2\text{-}OH)_2(\mu_3\text{-}OH)_4(\mu\text{-}OOCCH_3)_8(LH_2)_4]\cdot(OH)_2$ (**2**) is described herein, as a representative example, to illustrate the common structural features of these complexes. The structural details of complexes **1** and **3**–**6** are given in the Supporting Information (see Figure S1–S5).

The various aspects of the structural details of **2** are given in Figure 1a–f. The crystal structure of **2** reveals it to be a dicationic complex, $[Ni_4Gd_4(\mu_2\text{-}OH)_2(\mu_3\text{-}OH)_4(\mu\text{-}OOCCH_3)_8(LH_2)_4]^{2+}$, containing two counter hydroxide ions that are involved in a hydrogen-bonded interaction with the complex. The structure of the complex can be understood in the following way. The whole complex can be structurally decomposed into two $Ni^{II}_2Ln^{III}_2$ subunits, which are interconnected by hydroxide and acetate bridges. Two $[LH_2]^-$ units are involved in binding and assembling the $Ni^{II}_2Ln^{III}_2$ motifs. The two Ln^{III}s present in the sub unit are bridged to each other by a pair of hydroxide ligands affording a four-membered $Ln^{III}_2O_2$ ring. Each of the bridging OH groups is also involved in binding to a Ni^{II}. The phenolate unit of a $[LH_2]^-$ is involved in bridging Ni^{II} and Ln^{III} and is also involved in interaction with an additional Ni^{II}. The imino nitrogen and the free NH of the ethylenediamine motif are involved in a chelating coordination action to Ni^{II}. Interestingly, the $N\text{–}CH_2CH_2OH$ unit does not take part in coordination and is unutilized; however, the OH group is involved in a hydrogen bonding to the counter hydroxide ions (Figure 1a,b). Each of the methoxy groups on the aromatic scaffold are involved in a terminal coordination to the lanthanide ions. Finally, the two subunits are linked to each other by a pair of hydroxide ligands and four acetate ligands.

As a result of the cumulative coordination interaction described above, the complex contains two tetranuclear $Ni^{II}_2Ln^{III}_2O_4$ cubane cores (containing μ_2-acetate- and hydroxide ligands). As mentioned above, the acetate ligands bridge the Gd^{III} ions of two different cubane cores in a *syn–syn* $\mu\text{-}\eta^1\text{:}\eta^1$ fashion to form the heterometallic octanuclear core. A perspective view of the octanuclear core structure is shown in Figure 1c.

The Gd^{III} ions are all equivalent and have an 8O coordination environment in a trigonal dodecahedron geometry as confirmed by SHAPE analysis[40] (Figure 1e; Table S3 in the Supporting Information). Three oxygen atoms of the 8O coordination environment are from the bridging carboxylate groups (O2C, O2D, and O1E; Gd–O average distance 2.359(4) Å), three from hydroxide ligands (O1H, O2H, and O1G; Gd–O average distance 2.353(3) Å), and two O atoms (Gd–O1B distance 2.581(3) Å and Gd–O2B distance 2.482(3) Å) from the phenoxide motif of the ligand.

The Ni^{II} centers in the complex are equivalent and are hexacoordinate (2N, 4O) in a distorted octahedral geometry (Table S4 in the Supporting Information) with the nitrogen atoms occupying the cis positions (Figure 1f). The coordination sphere consists of two oxygen atoms from the phenolates of two different ligands (O2B and O2A; Ni–O average distance 2.140(3) Å), one oxygen atom from the hydroxide ligand (Ni–O1H distance 2.018(3) Å), one oxygen atom from the acetate ligand (Ni–O2E distance 2.083(3) Å), and two N atoms of the same ligand (N1B and N2B; average distance 2.060(4) Å). The average $Gd\text{–}O_{oph}\text{–}Ni$ bond angle is 98.35(10)°, while the average Ni···Gd separation is 3.502(6) Å. The dihedral angles in the bridging fragment were obtained through mean plane analysis shown in Figure 1d. The dihedral angle containing plane 1 (O2A–Gd2–O2H) and plane 2 (O2A–Ni1–O2H) is 16.0°; however, a value of 21.1° is obtained when plane 3 and plane 4 were considered.

We have also checked the phase purity of all the complexes (**1**–**6**) using powder X-ray diffraction analysis (Figures S8–S13 in the Supporting Information), which shows good agreement with the simulated patterns generated from the SCXRD data. Analysis of the crystal packing diagram reveals that the shortest distance between two Ln^{III} centers of the neighboring molecule is 9.714 Å (Figure S7).

Magnetic Properties. The temperature dependence of the $\chi_M T$ product for complexes **1**–**6** (χ_M being the molar magnetic susceptibility per mononuclear $Ni^{II}_4Ln^{III}_4$ unit) in the 2–300 K temperature range was measured with an applied magnetic field of 0.1 T and is given in Figures 2 and 3 for complexes **1** and **2**, respectively, and in Figure 6 for complexes **3**–**6**.

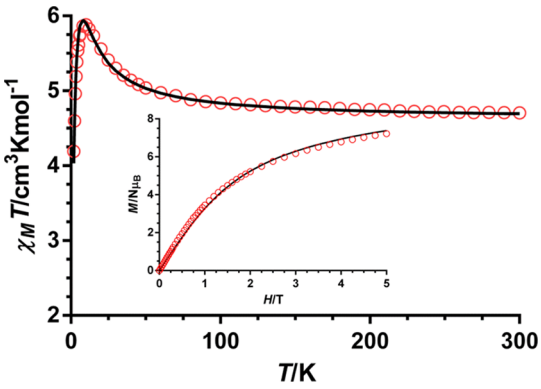

Figure 2. Temperature dependence of the $\chi_M T$ product and field dependence of magnetization for compound **1**. The solid lines represent the best fit of the experimental data.

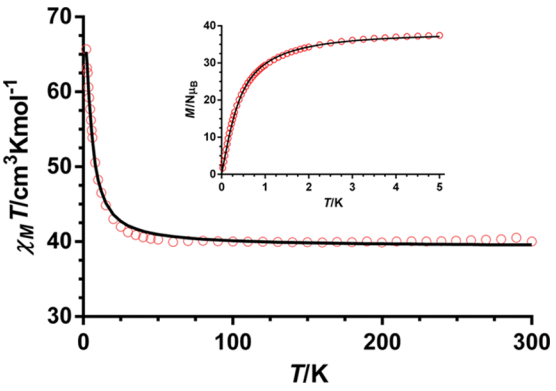

Figure 3. Temperature dependence of the $\chi_M T$ product and field dependence of magnetization for compound **2**. The solid lines represent the best fit of the experimental data.

At room temperature, the observed $\chi_M T$ values for **1**–**6** are close to those calculated for four independent Ni^{II} and Ln^{III} (Y^{III}) ions in the free ion approximation (Table 2). We are going to start the discussion with the Ni_4Y_4 (**1**) and Ni_4Gd_4 (**2**) complexes. On lowering the temperature, the $\chi_M T$ slowly increases from room temperature to 50 K (5.03 cm^3 K mol^{-1}) for **1** and 30 K (42.1 cm^3 K mol^{-1}) for **2** and then in a more abrupt way to reach values of 5.88 cm^3 K mol^{-1} at 10 K and

DOI: 10.1021/acsomega.8b00292
ACS Omega 2018, 3, 5202–5211

Table 2. Direct Current Magnetic Data for Complexes 1−6

compound	theoretical $\chi_M T_{300K}$ value (cm^3 K mol^{-1})	experimental $\chi_M T_{300K}/\chi_M T_{2K}$ (cm^3 K mol^{-1})	xperimental M_{sat} value (T = 2 K, H = 5 T) ($N\mu_B$)	theoretical M_{sat} value ($N\mu_B$)[b]
1	4.6 (g = 2.15)	4.7/4.19	7.21	8.6
2	39.1 (g = 2.10)	40.3/67.5	37.5	37.8
3	51.3[a]	52.5/98.3	25.9	44
4	60.7[a]	61.4/55.1	30.7	48
5	60.3[a]	61.6/36.2	31.0	48
6	49.9[a]	51.6/37.3	29.1	44

[a] $g_{Ni} = 2$; $\chi_M T = \frac{N\beta^2}{3k}\{g_J{}^2 J(J+1) + g_{Ni}{}^2 S(S+1)\}$.

[b] $M = NJ\mu_B$; $J = L + S$; $g_j = \frac{3}{2} + \frac{S_T(S_T+1) - L(L+1)}{2J(J+1)}$

65.7 cm^3 K mol^{-1} at 2 K, for **1** and **2**, respectively. These behaviors are due to a ferromagnetic interaction between the Ni^{II} ions in the case of **1** and between the Ni^{II} ions and the Ni^{II} and Gd^{III} ions in the case of **2**. In the case of **1**, the $\chi_M T$ decreases below 10 K up to 2 K, which is probably associated with the zero-field splitting effect of the Ni^{II} ions.

The magnetic properties of **1** have been modeled by using the following Hamiltonian:

$$H = -J(S_{Ni1}S_{Ni2} + S_{Ni1'}S_{Ni2'}) - J_a(S_{Ni1}S_{Ni2} + S_{Ni1'}S_{Ni2'}) + \sum_{i=1}^{4} D_{Nii}S_{Niiz}{}^2 \quad (1)$$

where J accounts for the magnetic exchange coupling between Ni^{II} ions, J_a represents the magnetic exchange coupling between Ni^{II} ions through the shorter Ni1−Y3−Y3′−Ni1′ and Ni2−Y4−Y4′−Ni2′ pathways, and D_{Ni} accounts for the axial single ion zero-field splitting parameter of the Ni^{II} ions, which are equivalent (see Figure 4). The simultaneous fit of the experimental susceptibility and magnetization data with the above Hamiltonian using the PHI program[41] afforded the following set of parameters: J = +5.2 cm^{-1}, J_a = −0.09 cm^{-1}, g = 2.15, D = 5.6 cm^{-1}, and R = 4.3 × 10^{-7}. The very weak antiferromagnetic (AF) interaction described by J_a must be taken into account, because when J_a is fixed to zero the quality of the fit got rather worse.

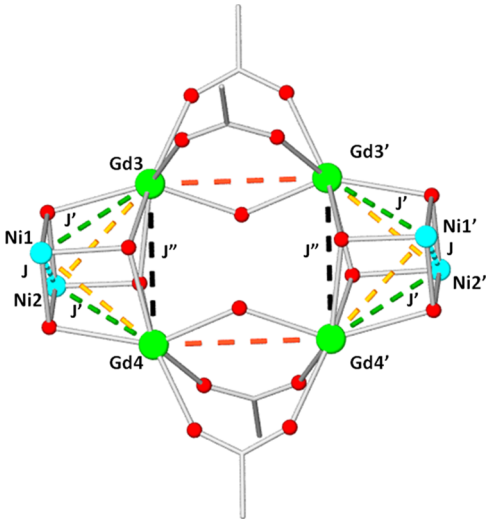

Figure 4. Scheme of the magnetic coupling pathways in complex **2**.

The ferromagnetic coupling exhibited by complex **1** can be justified by analyzing the structural parameters of dinuclear Ni_2 complexes with the diphenoxido bridging group connecting octahedral Ni^{II} ions. Experimental and theoretical magneto-structural correlations[42] have shown that the Ni−O−Ni bridging angle (θ) is the major issue influencing the nature of the magnetic coupling in hydroxido-, alkoxido-, and phenoxido-$Ni(O)_2Ni$ complexes. Thus, for Ni−O−Ni angles close to 90°, a ferromagnetic coupling is expected. As the Ni−O−Ni angle increases from 90°, the ferromagnetic coupling diminished and becomes AF at values of ∼96−98°. Moreover, it has been shown from theoretical studies[42a] that the AF interaction increases when τ (the out-of-plane displacement of the phenyl carbon atom from the Ni_2O_2 plane) diminishes. Taking into account this, the $Ni(O)_2Ni$ diphenoxo-bridging fragment in complex **1**, with mean θ and τ angles of 98.6° and 46.7° should transmit either weak F or AF interactions between the Ni^{2+} ions, which is in good agreement with the observed values.

The magnetic data for such an intricate as the Ni_4Gd_4 complex (**2**) were modeled in a crude manner with the following Hamiltonian

$$H = -J(S_{Ni1}S_{Ni2} + S_{Ni1'}S_{Ni2'}) - J'\sum_{i=1}^{8}(S_{Nii}S_{Gdi}) - J''(Gd_3Gd_4 + Gd_{3'}Gd_{4'}) + \sum_{i=1}^{8} D_{Nii}S_{Niiz}{}^2 - zJ'\langle S_z\rangle S_z \quad (2)$$

where the interactions between the Gd^{III} and Ni^{II} ions connected by two μ_3-O bridging atoms of the two cubane units are assumed to be equal, J'' represents the Gd−Gd interactions inside the cubane units, and zJ' accounts for the intercubane interactions between the Gd^{III} using the molecular field approach (see Figure 4). Taking into account that the structural parameters affecting the dinuclear Ni_2 units inside the cubane units are almost identical for the isostructural complexes **1** and **2** and to avoid over-parametrization, the values of J and D were fixed to those extracted for compound **1**. Considering the above approximations, the best fit of the magnetic data with the above Hamiltonian led to the following magnetic parameters: J' = 0.86 cm^{-1}, J'' = −0.0034 cm^{-1}, g = 2.10, zJ' = −0.0002 cm^{-1}, and R = 1.2 × 10^{-5}.

Experimental and theoretical studies on diphenoxide-bridged GdNi dinuclear complexes[43,44] have shown that the ferromagnetic interaction between Ni^{II} and Gd^{III} ions increases mainly with the increase of the Ni−O−Gd angle (θ) and with the planarity of the Ni−O_2−Gd fragment. Complex **2** has average values of the θ angle and the hinge angle β (the dihedral angle between the O−Ni−O and O−Gd−O planes in the bridging fragment) of 102.1° and 18.6°, respectively. For these values and according to the magnetostructural correlations, a $J_{NiGd} \approx +1$ cm^{-1} is expected, which agrees well with the J'_{NiGd} value extracted for **2**. It is worth noting that the magnetic coupling constants for the Ni···Gd and Gd···Gd intracubane interactions agree in sign and magnitude with those found for other $Ni_2Gd_2O_4$ cubane complexes.[45] As the Gd^{III} ion has no first order angular momentum and almost a negligible zero-field splitting, the dipolar interactions are expected to be very weak, so that the experimentally observed Gd···Gd interactions are due mainly to exchange coupling between the Gd^{III} ions. Experimental and theoretical studies have shown that for

DOI: 10.1021/acsomega.8b00292
ACS Omega 2018, 3, 5202−5211

diphenoxo- and dialkoxo-, two oxo-carboxylate and two carboxylate-acetate bridging groups seem to indicate that the smaller values of the Gd−O−Gd, and consequently the Gd···Gd distance, favor the AF interaction.[46] For some of these compounds, AF interactions are predicted for Gd−O−Gd angles smaller than 110°. In view of the above considerations, the fact that the intracubane AF interactions (described by J'') are larger than the intercubane ones (described by zJ') is not unexpected as the Gd−O−Gd angles for the former are around 108.5°, whereas the Gd−O−Gd angle for the latter ones is 132.23°. Taking into account only the Gd−O−Gd angle, the intercubane interaction is expected to be ferromagnetic in nature; however, the existence of two additional *syn*−*syn* acetate bridging groups connecting the Gd^{III} ions lead to the very weak AF interaction found for this triple bridge. Nevertheless, these assumptions should be taken with caution because of (i) the crudeness of the model, (ii) the weakness of the magnetic interactions, and (iii) the possible existence of ZFS splitting of the Gd^{III} ions.

Previous work has shown that Ni_xGd_y polynuclear complexes can exhibit large magneto-caloric effects (MCE) and therefore can be considered for magnetic refrigeration materials.[47] This is so because, among other factors, the magnetic exchange interaction between the Gd^{III} and Ni^{II} ions is very weak, which generates multiple low-lying excited and field-accessible states, each of which can contribute to the total magnetic entropy of the system. Moreover, if the interaction is ferromagnetic in nature, the low-lying states would have a large spin, which also favors a larger MCE. In view of this, we decided to evaluate the MCE of **2** from magnetization measurements in the 2−6 K temperature range under an applied magnetic field in the range 0−5 T, making use of the Maxwell relation

$$\Delta S_m = (T, \Delta B) = \int_{B_i}^{B_f} \left[\frac{\partial M(T, B)}{dT}\right]_B dB \quad (3)$$

where B_i and B_f are the initial and final applied magnetic fields. The integration results show that the $-\Delta S_m$ values for complex **2** under all fields (Figure 5) increase as the temperature decreases from 5 to 3 K, with a maximum magnetic entropy change ($-\Delta S_m$ = 22.58 J kg^{-1} K^{-1}). This value is rather smaller than the full magnetic entropy content per mole for the $Ni_4^{II}Gd_4^{III}$ complex is $2R\ \ln(2S_{Gd} + 1) + 2R\ \ln(2S_{Ni} + 1) = 6.08R$, which corresponds to 36.8 J kg^{-1} K^{-1} for **2**. This fact can be mainly due to magnetic anisotropy of the Ni^{II} ions and the intra- and intercubane AF interactions between the Gd^{III} ions (both the increase of D and AF interactions diminishes $-\Delta S_m$). The $-\Delta S_m$ value for **2** is larger than those observed for complexes with a Gd/Ni = 0.5 but lower than those found for other more dense complexes with Gd/Ni ratios in the range 1−4.2.[47] The MCE increases with the increase of the Gd/Ni ratio as expected for increasing the spin and decreasing the magnetic anisotropy.

The $\chi_M T$ product of compounds Ni_4Tb_4 (**3**) and Ni_4Dy_4 (**4**) steadily decreases with decreasing temperature to minimum values of 49.1 cm^3 K mol^{-1} at 35 K for **3** and 54.74 cm^3 K mol^{-1} at 12 K for **4** and then sharply increases at lower temperatures up to 2 K in the case of **3** and to reach a maximum value of 55.5 cm^3 K mol^{-1} at 5 K for **4**. Below this temperature, the $\chi_M T$ value for **4** drops down to 2 K. As usual, the decrease of the $\chi_M T$ product in the high temperature region (above 40 K) is due to the depopulation of the M_J sublevels of the Tb^{III} and Dy^{III} ions, which arise from the splitting of the ground term by the ligand field. The increase of $\chi_M T$ at low temperature is likely to be due to a ferromagnetic interaction between Ni^{II} and Ln^{III}, whereas the decrease of $\chi_M T$ below 5 K for **4** is essentially associated with the magnetic anisotropy of the Ni^{II} ions. For complexes **5** and **6**, the $\chi_M T$ product decreases steadily with decreasing temperature until approximately 20 K and then more sharply down to 2 K. The observed behavior is mainly due to the depopulation of the M_J sublevels of the Ln^{III} ions, which are able to overcome (together with the effect of the Ni^{II} anisotropy) the effect of the presumable Ni^{II}−Ln^{III} ferromagnetic interactions in the low temperature region. This behavior is rather common in Ho^{III} and Er^{III} complexes. In the case of complexes **3** and **4**, the opposite situation occurs, so that the Ni^{II}−Ln^{III} ferromagnetic interactions are strong enough as to overcome the effect of the depopulation of the M_J sublevels, and an increase in $\chi_M T$ is observed at a low temperature. The fact that the $\chi_M T$ for **3** reaches a rather larger value than **4** at 2 K seems to indicate that the Ni^{II}−Ln^{III} magnetic coupling is stronger for the former.

The magnetization versus field plots for complexes **3**−**6** at T = 2 K (Figure 6) show a fast increase of the magnetization up to ∼1 T, which supports the ferromagnetic interaction between Ni^{II} and Ln^{III} in these complexes, and then a slow increase with the field without reaching saturation at 5 T, which is mainly due

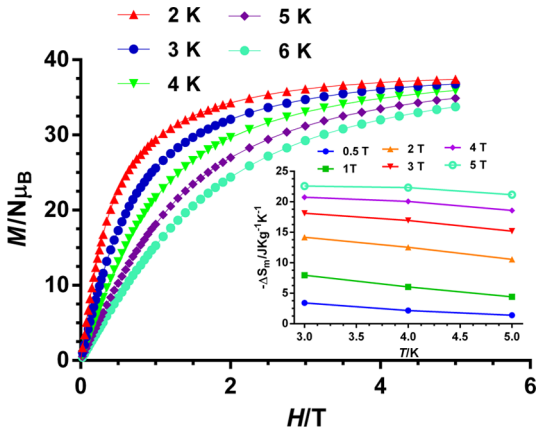

Figure 5. Isothermal field-dependent curves for **2** between 2 and 6 K and magnetic entropy changes (inset) extracted from the experimental magnetization data with the Maxwell equation between 1 and 5 T and temperatures from 3 to 5 K (points).

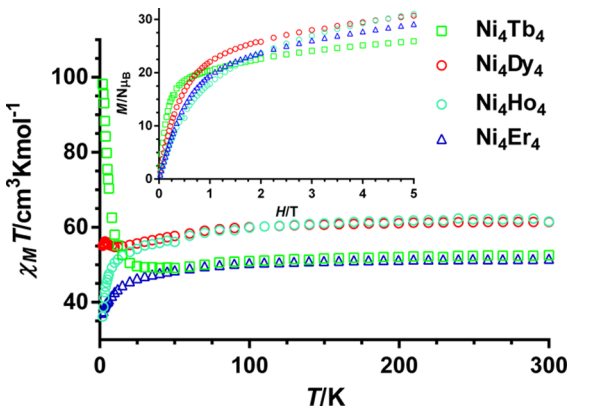

Figure 6. Temperature dependence of the $\chi_M T$ product and field dependence of magnetization (inset) for compounds **3**−**6**.

DOI: 10.1021/acsomega.8b00292
ACS Omega 2018, 3, 5202−5211

to the presence of significant magnetic anisotropy and/or low-lying excited states that are partially populated at this temperature. The presence of low-lying excited states is in agreement with the existence of weak Ni−Ln magnetic interactions in these complexes. It should be noted that the magnetization values at the highest applied dc magnetic field of 5 T are however almost the half of those calculated for non-interacting Ni^{II} and Ln^{III} ions (Table 2), which is, as usual, mainly attributed to crystal-field effects giving rise to significant magnetic anisotropy.[48] The fact that the slope of the M versus H plot below 1 T is higher for **3** than for **4** seems to support a stronger Ni^{II}−Ln^{III} magnetic coupling for the former. The smaller slope for **5** and **6** could indicate a weaker magnetic coupling than in complexes **3** and **4**. Nevertheless, these qualitative suggestions should be taken with caution as the crystal field splitting of the ground term by the ligand field is different for each of the complexes **3**−**6** and therefore their ability for counterbalancing the effect of the Ni^{II}−Ln^{III} ferromagnetic coupling.

To know if these complexes exhibit slow relaxation and possible SMM behavior, dynamic ac magnetic susceptibility measurements as a function of the temperature at different frequencies were performed on complexes **1**−**6** under zero and 1000 Oe external dc field. Only complexes **3** and **4** showed out-of-phase (χ''_M) signals below 4 K (Figure S15), but none of them exhibited any maximum in the temperature dependence of χ''_M above 2 K at frequencies reaching 1400 Hz, even in the presence of a small dc field to fully or partly suppress the possible quantum tunneling relaxation (this process is able in some cases to prevent the observation of slow relaxation of the magnetization). Therefore, in these two complexes either the energy barrier for the flipping of the magnetization is not enough as to block the magnetization above 2 K or there exists a very fast resonant zero-field quantum tunneling of the magnetization (which cannot be eliminated by applying a small dc field) with a flipping rate that is too fast to give rise to a maximum in the χ''_M above 2 K. This behavior can be related to the existence of very weak Ni···Ln and Ln···Ln magnetic interactions in complexes **3**−**6**. These interactions generate small separations of the low-lying split sublevels, which lead to very small energy barrier for the flipping of the magnetization and, moreover, favor QTM by mixing of low-lying excited states in the ground state.

Summary. A compartmental ligand, 2-methoxy-6-[{2-(2-hydroxyethylamino)ethylimino}methyl]phenol (LH_3), was utilized to assemble heterometallic octanuclear Ni_4Ln_4 complexes. Structural studies of these complexes reveal that they are made up of two tetranuclear $[Ni_2Ln_2O_4]$ cubane subunits. The core of the assembly consists of a tetranuclear lanthanide motif, where two four-membered $[Ln_2(\mu\text{-}OH)_2]$ subunits are linked to each other by four acetate and two hydroxide bridging ligands. Magnetic studies on these complexes reveal a ferromagnetic interaction between the lanthanide and the nickel centers, the magnitude of which for the Gd^{III} analogue has been estimated as J = + 0.86 cm^{-1}. While none of the complexes are SMMs because of the existence of very weak Ni···Ln and Ln···Ln magnetic interactions, the $Ni^{II}_4Gd^{III}_4$ complex shows a magneto-caloric effect with a maximum magnetic entropy change, $-\Delta S_m$ = 22.58 J kg^{-1} K^{-1} at 3 K for an applied external field of 5 T.

EXPERIMENTAL SECTION

Materials and Methods. Solvents and other general reagents used in this work were purified according to standard procedures.[49,50] *o*-Vanillin, nickel acetate tetrahydrate, and tetramethyl ammonium hydroxide pentahydrate were obtained from Spectrochem Pvt. Ltd., Mumbai, India. *N*-(2-Hydroxyethyl)ethylenediamine and $Ln(NO_3)_3{\cdot}xH_2O$ (x = 6, for Ln = Y and Gd; x = 5 for Ln = Dy, Tb, Ho, and Er) were obtained from Sigma Aldrich Chemical Co. (USA). All these chemicals were used as obtained without further purification. The ligand 2-methoxy-6-[2{-(2-hydroxyethylamino)-ethylimino}methyl]phenol (LH_3) was prepared following a previously reported procedure.[51,52]

Instrumentation. Melting points were measured using a JSGW melting point apparatus and are uncorrected. IR spectra were recorded with a PerkinElmer Fourier transform infrared spectrometer. Mass spectra were recorded with a Bruker micrOTOF-Q II spectrometer. Powder X-ray diffraction data of all the complexes were collected with a Bruker D8 ADVANCE X-ray powder diffractometer using Cu Kα radiation (λ = 1.5418 Å). Elemental analyses of the compounds were obtained from a Euro Vector EA instrument (CHNS-O, model EuroEA3000). Thermogravimetric analysis (TGA) was carried out by TA Instrument (model: Discovery TGA).

Magnetic Measurements. Static magnetic properties were measured on polycrystalline samples of the complexes in the temperature range 2−300 K under an applied field of 1000 Oe using a Quantum Design SQUID MPMS XL-5 magnetometer. Field dependence of the dynamic (ac) susceptibility measurements were carried out using an alternating ac field of 3.5 Oe in the frequency range 1−1500 Hz. The static experimental susceptibilities were corrected for the diamagnetism of the constituent atoms (using Pascal's constants) and for the sample holder. To avoid any torquing of the microcrystals, a pellet of the sample cut into very small fragments was introduced in the sample holder.

X-ray Crystallography. Single-crystal X-ray structural studies of **1**−**6** were performed on a Bruker APEX II CCD diffractometer equipped with graphite-monochromated Mo Kα radiation (λ_α = 0.71073 Å) at 100(2) K. The crystals did not degrade/decompose during data collection. The frames were indexed, integrated, and scaled using the SMART and SAINT software package.[53] Absorption correction was performed by a multiscan method implemented in SADABS.[54] Space groups were determined using XPREP implemented in APEX2.[55] The structures were solved with the ShelXT[56] structure solution program using intrinsic phasing and refined with the ShelXL[57] refinement package using least squares minimization in the Olex2[58] software. All the nonhydrogen atoms were refined with anisotropic thermal parameters. All the hydrogen atoms except the bridging −OH atoms were included in idealized positions, and a riding model was used. Lattice solvent molecules could not be satisfactorily modeled by the present analysis because of heavy disorder associated with it. Therefore, the "PLATON/SQUEEZE" program[59] was used to remove those disordered solvent molecules. All the mean plane analyses and crystallographic figures have been generated using the DIAMOND software (version 3.2).[60]

Synthesis of Complexes 1−6. The general synthetic protocol that was used for the preparation of the metal complexes (**1**−**6**) is as follows: a methanolic solution (5 mL) of $Ln(NO_3)_3{\cdot}xH_2O$ (1 eq) (where x = 6 for **1** and **2**, and x = 5 for

DOI: 10.1021/acsomega.8b00292
ACS Omega 2018, 3, 5202−5211

3−**6**) was added dropwise to a 15 mL methanolic solution containing a mixture of LH_3 (1 eq) and tetramethyl ammonium hydroxide (2 eq) with constant stirring. To this reaction mixture, solid $Ni(CH_3COO)_2{\cdot}4H_2O$ (1 eq) was added and the resulting deep orange-colored solution stirred further for 12 h. The volume of the solution was reduced to ∼10 mL by rotary evaporation, filtered, and kept undisturbed for crystallization under ambient conditions. Slow evaporation of the solvent afforded green, block-shaped crystals suitable for X-ray analysis after 2 weeks. The stoichiometry of the reactants involved in each reaction, the yield of the products, and their characterization data are provided below:

*$[Ni_4Y_4(\mu_2\text{-}OH)_2(\mu_3\text{-}OH)_4(\mu\text{-}OOCCH_3)_8(LH_2)_4]{\cdot}(OH)_2{\cdot}4H_2O$ (**1**).* LH_3 (0.050 g, 0.209 mmol), $Y(NO_3)_3{\cdot}6H_2O$ (0.094 g, 0.209 mmol), $Ni(CH_3COO)_2{\cdot}4H_2O$ (0.052 g, 0.209 mmol), and $Me_4NOH{\cdot}5H_2O$ (0.076 g, 0.419 mmol) were used. Yield: 0.051 g, 41.80% (based on Y). mp: >230 °C. IR (KBr ν/cm^{-1}): 3404 (br), 2943 (m), 2881 (w), 1655 (s), 1613 (s), 1573 (s), 1434 (s), 1381 (s), 1267 (s), 1224 (s), 1173 (w), 1142 (w), 1075 (s), 1041 (m), 985 (w), 954 (m), 846 (w), 784 (w), 745 (s), 655 (m), 615 (w), 541 (w), 515 (w), 426 (m). Anal. Calcd (%) for $C_{64}H_{108}Y_4N_8Ni_4O_{40}$: C, 34.63; H, 4.90; N, 5.05. Found: C, 34.41; H, 4.76; N, 4.88.

*$[Ni_4Gd_4(\mu_2\text{-}OH)_2(\mu_3\text{-}OH)_4(\mu\text{-}OOCCH_3)_8(LH_2)_4]{\cdot}(OH)_2{\cdot}H_2O$ (**2**).* LH_3 (0.050 g, 0.209 mmol), $Gd(NO_3)_3{\cdot}6H_2O$ (0.094 g, 0.209 mmol), $Ni(CH_3COO)_2{\cdot}4H_2O$ (0.052 g, 0.209 mmol), and $Me_4NOH{\cdot}5H_2O$ (0.076 g, 0.419 mmol) were used. Yield: 0.035 g, 46.05% (based on Gd). mp: >230 °C. IR (KBr ν/cm^{-1}): 3402 (br), 2946 (m), 2880 (w), 1653 (s), 1612 (s), 1572 (s), 1434 (s), 1384 (s), 1268 (s), 1224 (s), 1170 (w), 1139 (w), 1073 (s), 1041 (m), 984 (w), 954 (m), 849 (w), 787 (w), 746 (s), 657 (m), 615 (w), 542 (w), 512 (w), 424 (m). Anal. Calcd (%) for $C_{64}H_{102}Gd_4N_8Ni_4O_{37}$: C, 31.51; H, 4.21; N, 4.59. Found: C, 31.35; H, 4.08; N, 4.41.

*$[Ni_4Tb_4(\mu_2\text{-}OH)_2(\mu_3\text{-}OH)_4(\mu\text{-}OOCCH_3)_8(LH_2)_4]{\cdot}(OH)_2{\cdot}5H_2O$ (**3**).* LH_3 (0.050 g, 0.209 mmol), $Tb(NO_3)_3{\cdot}6H_2O$ (0.091 g, 0.209 mmol), $Ni(CH_3COO)_2{\cdot}4H_2O$ (0.052 g, 0.209 mmol), and $Me_4NOH{\cdot}5H_2O$ (0.076 g, 0.419 mmol) were used. Yield: 0.042 g, 48.64% (based on Tb). mp: >230 °C. IR (KBr ν/cm^{-1}): 3401 (br), 2945 (m), 2881 (w), 1656 (s), 1610 (s), 1570 (s), 1433 (s), 1384 (s), 1268 (s), 1223 (s), 1173 (w), 1140 (w), 1070 (s), 1040 (m), 986 (w), 953 (m), 848 (w), 784 (w), 749 (s), 659 (m), 616 (w), 540 (w), 511 (w), 423 (m). Anal. Calcd (%) for $C_{64}H_{110}Tb_4N_8Ni_4O_{41}$: C, 30.53; H, 4.40; N, 4.45. Found: C, 30.26; H, 4.17; N, 4.20.

*$[Ni_4Dy_4(\mu_2\text{-}OH)_2(\mu_3\text{-}OH)_4(\mu\text{-}OOCCH_3)_8(LH_2)_4]{\cdot}(OH)_2{\cdot}6H_2O$ (**4**).* LH_3 (0.050 g, 0.209 mmol), $Dy(NO_3)_3{\cdot}5H_2O$ (0.092 g, 0.209 mmol), $Ni(CH_3COO)_2{\cdot}4H_2O$ (0.052 g, 0.209 mmol), and $Me_4NOH{\cdot}5H_2O$ (0.076 g, 0.419 mmol) were used. Yield: 0.041 g, 53.67% (based on Dy). mp: >230 °C. IR (KBr ν/cm^{-1}): 3401 (br), 2947 (m), 2884 (w), 1657 (s), 1610 (s), 1570 (s), 1433 (s), 1384 (s), 1268 (s), 1225 (s), 1172 (w), 1140 (w), 1075 (s), 1039 (m), 986 (w), 955 (m), 848 (w), 789 (w), 744 (s), 657 (m), 614 (w), 541 (w), 514 (w), 425 (m). Anal. Calcd (%) for $C_{64}H_{112}Dy_4N_8Ni_4O_{42}$: C, 30.14; H, 4.43; N, 4.39. Found: C, 29.86; H, 4.59; N, 4.11.

*$[Ni_4Ho_4(\mu_2\text{-}OH)_2(\mu_3\text{-}OH)_4(\mu\text{-}OOCCH_3)_8(LH_2)_4]{\cdot}(OH)_2{\cdot}6H_2O$ (**5**).* LH_3 (0.050 g, 0.209 mmol), $Ho(NO_3)_3{\cdot}5H_2O$ (0.092 g, 0.209 mmol), $Ni(CH_3COO)_2{\cdot}4H_2O$ (0.052 g, 0.209 mmol), and $Me_4NOH{\cdot}5H_2O$ (0.076 g, 0.419 mmol) were used. Yield: 0.040 g, 52.60% (based on Ho). mp: >230 °C. IR (KBr ν/cm^{-1}): 3403 (br), 2946 (m), 2879 (w), 1652 (s), 1614 (s), 1576 (s), 1432 (s), 1384 (s), 1268 (s), 1225 (s), 1172 (w), 1138 (w), 1075 (s), 1039 (m), 983 (w), 955 (m), 850 (w), 786 (w), 744 (s), 660 (m), 614 (w), 541 (w), 514 (w), 426 (m). Anal. Calcd (%) for $C_{64}H_{112}Ho_4N_8Ni_4O_{42}$: C, 30.03; H, 4.41; N, 4.38. Found: C, 29.77; H, 4.20; N, 4.08.

*$[Ni_4Er_4(\mu_2\text{-}OH)_2(\mu_3\text{-}OH)_4(\mu\text{-}OOCCH_3)_8(LH_2)_4]{\cdot}(OH)_2{\cdot}4H_2O$ (**6**).* LH_3 (0.050 g, 0.209 mmol), $Er(NO_3)_3{\cdot}5H_2O$ (0.093 g, 0.209 mmol), $Ni(CH_3COO)_2{\cdot}4H_2O$ (0.052 g, 0.209 mmol), and $Me_4NOH{\cdot}5H_2O$ (0.076 g, 0.419 mmol) were used. Yield: 0.044 g, 57.08% (based on Er). mp: >230 °C. IR (KBr ν/cm^{-1}): 3414 (br), 2944 (m), 2881 (w), 1656 (s), 1611 (s), 1573 (s), 1435 (s), 1384 (s), 1267 (s), 1225 (s), 1169 (w), 1139 (w), 1073 (s), 1041 (m), 983 (w), 955 (m), 848 (w), 786 (w), 743 (s), 658 (m), 618 (w), 542 (w), 513 (w), 427 (m). Anal. Calcd (%) for $C_{64}H_{108}Er_4N_8Ni_4O_{40}$: C, 30.34; H, 4.30; N, 4.42. Found: C, 30.06; H, 4.11; N, 4.21.

■ ASSOCIATED CONTENT

Supporting Information

The Supporting Information is available free of charge on the ACS Publications website at DOI: 10.1021/acsomega.8b00292.

CCDC 1586139 (**1**), 1581911 (**2**), 1581909 (**3**), 1581902 (**4**), 1581920 (**5**), and 1581912 (**6**) contain crystallographic supplementary data for this paper. These data can be obtained free of charge from The Cambridge Crystallographic Data Centre via www.ccdc.cam.ac.uk/data_request/cif (CIF)

Molecular structures of complexes **1** and **3**−**6**; coordination modes of ligands; crystal packing diagram of complex **2**; BVS calculation; powder X-ray diffraction patterns of complexes **1**−**6**; TGA curves of complexes **1**−**6**; temperature dependence of the in-phase and out-of-phase susceptibility plot; hydrogen bonding parameters for complexes **1**−**6**; continuous shape measures calculations; and detailed crystallographic data for complexes **1**−**6** (PDF)

■ AUTHOR INFORMATION

Corresponding Authors

*E-mail: ecolacio@ugr.es (E.C.).

*E-mail: vc@iitk.ac.in or vc@tifrh.res.in (V.C.).

ORCID

Pankaj Kalita: 0000-0002-1240-5633

Juan Manuel Herrera: 0000-0002-9255-227X

Vadapalli Chandrasekhar: 0000-0003-1968-2980

Notes

The authors declare no competing financial interest.

■ ACKNOWLEDGMENTS

V.C. is thankful to the Department of Science and Technology, New Delhi, India, for a National J. C. Bose Fellowship. P.K. and J.G. are thankful to the National Institute of Science Education and Research, Bhubaneswar, for doctoral and postdoctoral fellowship, respectively. J.M.H. and E.C. are grateful to Ministerio de Economía y Competitividad (MINECO) and EU Feder Funds (Project CTQ2014-56312-P), the Junta de Andalucía (FQM-195 and the Project of Excellence P11-FQM-7756), and the University of Granada for financial support.

■ REFERENCES

(1) Caneschi, A.; Gatteschi, D.; Sessoli, R.; Barra, A. L.; Brunel, L. C.; Guillot, M. Alternating Current Susceptibility, High Field Magnet-

DOI: 10.1021/acsomega.8b00292
ACS Omega 2018, 3, 5202−5211

ization, and Millimeter Band EPR Evidence for a Ground S = 10 State in $[Mn_{12}O_{12}(CH_3COO)_{16}(H_2O)_4].2CH_3COOH.4H_2O$. *J. Am. Chem. Soc.* **1991**, *113*, 5873−5874.
(2) Sessoli, R.; Tsai, H. L.; Schake, A. R.; Wang, S.; Vincent, J. B.; Folting, K.; Gatteschi, D.; Christou, G.; Hendrickson, D. N. High-Spin Molecules: $[Mn_{12}O_{12}(O_2CR)_{16}(H_2O)_4]$. *J. Am. Chem. Soc.* **1993**, *115*, 1804−1816.
(3) Sessoli, R.; Gatteschi, D.; Caneschi, A.; Novak, M. A. Magnetic Bistability in a Metal-Ion Cluster. *Nature* **1993**, *365*, 141−143.
(4) Christou, G.; Gatteschi, D.; Hendrickson, D. N.; Sessoli, R. Single-Molecule Magnets. *MRS Bull.* **2000**, *25*, 66−71.
(5) Heersche, H. B.; de Groot, Z.; Folk, J. A.; van der Zant, H. S. J.; Romeike, C.; Wegewijs, M. R.; Zobbi, L.; Barreca, D.; Tondello, E.; Cornia, A. Electron Transport through Single Mn12 Molecular Magnets. *Phys. Rev. Lett.* **2006**, *96*, 206801.
(6) Waldmann, O. A Criterion for the Anisotropy Barrier in Single-Molecule Magnets. *Inorg. Chem.* **2007**, *46*, 10035−10037.
(7) Neese, F.; Pantazis, D. A. What Is Not Required to Make a Single Molecule Magnet. *Faraday Discuss.* **2011**, *148*, 229−238.
(8) Frost, J. M.; Harriman, K. L. M.; Murugesu, M. The Rise of 3-D Single-Ion Magnets in Molecular Magnetism: Towards Materials from Molecules? *Chem. Sci.* **2016**, *7*, 2470−2491.
(9) Ako, A. M.; Hewitt, I. J.; Mereacre, V.; Clérac, R.; Wernsdorfer, W.; Anson, C. E.; Powell, A. K. A Ferromagnetically Coupled Mn_{19} Aggregate with a Record S = 83/2 Ground Spin State. *Angew. Chem., Int. Ed.* **2006**, *45*, 4926−4929.
(10) Wang, W.-G.; Zhou, A.-J.; Zhang, W.-X.; Tong, M.-L.; Chen, X.-M.; Nakano, M.; Beedle, C. C.; Hendrickson, D. N. Giant Heterometallic $Cu_{17}Mn_{28}$ Cluster with Td Symmetry and High-Spin Ground State. *J. Am. Chem. Soc.* **2007**, *129*, 1014−1015.
(11) Scott, R. T. W.; Parsons, S.; Murugesu, M.; Wernsdorfer, W.; Christou, G.; Brechin, E. K. Linking Centered Manganese Triangles into Larger Clusters: A {Mn32} Truncated Cube. *Angew. Chem., Int. Ed.* **2005**, *44*, 6540−6543.
(12) Ruiz, E.; Cirera, J.; Cano, J.; Alvarez, S.; Loose, C.; Kortus, J. Can Large Magnetic Anisotropy and High Spin Really Coexist? *Chem. Commun.* **2008**, 52−54.
(13) Cirera, J.; Ruiz, E.; Alvarez, S.; Neese, F.; Kortus, J. How to Build Molecules with Large Magnetic Anisotropy. *Chem.—Eur. J.* **2009**, *15*, 4078−4087.
(14) Wang, B.; Jiang, S.; Wang, X.; Gao, S. Magnetic Molecular Materials with Paramagnetic Lanthanide Ions. *Sci. China, Ser. B: Chem.* **2009**, *52*, 1739−1758.
(15) Rinehart, J. D.; Long, J. R. Exploiting Single-Ion Anisotropy in the Design of f-Element Single-Molecule Magnets. *Chem. Sci.* **2011**, *2*, 2078.
(16) Woodruff, D. N.; Winpenny, R. E. P.; Layfield, R. A. Lanthanide Single-Molecule Magnets. *Chem. Rev.* **2013**, *113*, 5110−5148.
(17) Tang, J.; Zhang, P. Lanthanide. A basis for Lanthanide Single-Molecule Magnets. In *Lanthanide Single Molecule Magnets*, 1st Ed; Springer-Verlag Berlin Heidelberg, 2015; pp 1−34.
(18) Blagg, R. J.; Ungur, L.; Tuna, F.; Speak, J.; Comar, P.; Collison, D.; Wernsdorfer, W.; McInnes, E. J. L.; Chibotaru, L. F.; Winpenny, R. E. P. Magnetic Relaxation Pathways in Lanthanide Single-Molecule Magnets. *Nat. Chem.* **2013**, *5*, 673−678.
(19) Langley, S. K.; Chilton, N. F.; Ungur, L.; Moubaraki, B.; Chibotaru, L. F.; Murray, K. S. Heterometallic Tetranuclear $[Ln^{III}_2Co^{III}_2]$ Complexes Including Suppression of Quantum Tunneling of Magnetization in the $[Dy^{III}_2Co^{III}_2]$ Single Molecule Magnet. *Inorg. Chem.* **2012**, *51*, 11873−11881.
(20) Liu, J.-L.; Wu, J.-Y.; Chen, Y.-C.; Mereacre, V.; Powell, A. K.; Ungur, L.; Chibotaru, L. F.; Chen, X.-M.; Tong, M.-L. A Heterometallic Fe^{II}-Dy^{III} Single-Molecule Magnet with a Record Anisotropy Barrier. *Angew. Chem., Int. Ed.* **2014**, *53*, 12966−12970.
(21) Langley, S. K.; Wielechowski, D. P.; Vieru, V.; Chilton, N. F.; Moubaraki, B.; Abrahams, B. F.; Chibotaru, L. F.; Murray, K. S. A {CrIII2DyIII2} Single-Molecule Magnet: Enhancing the Blocking Temperature through 3d Magnetic Exchange. *Angew. Chem., Int. Ed.* **2013**, *52*, 12014−12019.
(22) Gupta, T.; Beg, M. F.; Rajaraman, G. Role of Single-Ion Anisotropy and Magnetic Exchange Interactions in Suppressing Zero-Field Tunnelling in {3d-4f} Single Molecule Magnets. *Inorg. Chem.* **2016**, *55*, 11201−11215.
(23) Langley, S. K.; Le, C.; Ungur, L.; Moubaraki, B.; Abrahams, B. F.; Chibotaru, L. F.; Murray, K. S. Heterometallic 3d-4f Single-Molecule Magnets: Ligand and Metal Ion Influences on the Magnetic Relaxation. *Inorg. Chem.* **2015**, *54*, 3631−3642.
(24) Papatriantafyllopoulou, C.; Wernsdorfer, W.; Abboud, K. A.; Christou, G. $Mn_{21}Dy$ Cluster with a Record Magnetization Reversal Barrier for a Mixed 3d/4f Single-Molecule Magnet. *Inorg. Chem.* **2011**, *50*, 421−423.
(25) Chandrasekhar, V.; Pandian, B. M.; Vittal, J. J.; Clérac, R. Synthesis, Structure, and Magnetism of Heterobimetallic Trinuclear Complexes {$[L_2Co_2Ln][X]$}[Ln = Eu, X = Cl; Ln = Tb, Dy, Ho, X = NO 3;; LH 3 = (S)P[N(Me)N=CH-C6H3-2-OH-3-OMe]3]: A 3d-4f Family of Single-Molecule Magnets. *Inorg. Chem.* **2009**, *48*, 1148−1157.
(26) Das, S.; Bejoymohandas, K. S.; Dey, A.; Biswas, S.; Reddy, M. L. P.; Morales, R.; Ruiz, E.; Titos-Padilla, S.; Colacio, E.; Chandrasekhar, V. Amending the Anisotropy Barrier and Luminescence Behavior of Heterometallic Trinuclear Linear $[M^{II}$-Ln^{III}-$M^{II}]$ (Ln^{III}=Gd, Tb, Dy; M^{II}=Mg/Zn) Complexes by Change from Divalent Paramagnetic to Diamagnetic Metal Ions. *Chem.—Eur. J.* **2015**, *21*, 6449−6464.
(27) Goura, J.; Colacio, E.; Herrera, J. M.; Suturina, E. A.; Kuprov, I.; lan, Y.; Wernsdorfer, W.; Chandrasekhar, V. Heterometallic Zn3Ln3 Ensembles Containing (μ6-CO3) Ligand and Triangular Disposition of Ln^{3+} Ions: Single-Molecule Toroic (SMT) and Single-Molecule Magnet (SMM) Behavior. *Chem.—Eur. J.* **2017**, *23*, 16621.
(28) Ahmed, N.; Das, C.; Vaidya, S.; Langley, S. K.; Murray, K. S.; Shanmugam, M. Nickel(II)-Lanthanide(III) Magnetic Exchange Coupling Influencing Single-Molecule Magnetic Features in $\{Ni_2Ln_2\}$ Complexes. *Chem.—Eur. J.* **2014**, *20*, 14235−14239.
(29) Chen, W.-P.; Liao, P.-Q.; Yu, Y.; Zheng, Z.; Chen, X.-M.; Zheng, Y.-Z. A Mixed-Ligand Approach for a Gigantic and Hollow Heterometallic Cage $\{Ni_{64}RE_{96}\}$ for Gas Separation and Magnetic Cooling Applications. *Angew. Chem., Int. Ed.* **2016**, *55*, 9375−9379.
(30) Pasatoiu, T. D.; Ghirri, A.; Madalan, A. M.; Affronte, M.; Andruh, M. Octanuclear $[Ni^{II}_4Ln^{III}_4]$ Complexes. Synthesis, Crystal Structures and Magnetocaloric Properties. *Dalton Trans.* **2014**, *43*, 9136.
(31) Liu, D.-P.; Lin, X.-P.; Zhang, H.; Zheng, X.-Y.; Zhuang, G.-L.; Kong, X.-J.; Long, L.-S.; Zheng, L.-S. Magnetic Properties of a Single-Molecule Lanthanide-Transition-Metal Compound Containing 52 Gadolinium and 56 Nickel Atoms. *Angew. Chem., Int. Ed.* **2016**, *55*, 4532−4536.
(32) Biswas, S.; Goura, J.; Das, S.; Topping, C. V.; Brambleby, J.; Goddard, P. A.; Chandrasekhar, V. Octanuclear Heterobimetallic {Ni4Ln4} Assemblies Possessing Ln_4 Square Grid [2×2] Motifs: Synthesis, Structure, and Magnetism. *Inorg. Chem.* **2016**, *55*, 8422−8436.
(33) Goura, J.; Mereacre, V.; Novitchi, G.; Powell, A. K.; Chandrasekhar, V. Homometallic Fe^{III}_4 and Heterometallic $\{Fe^{III}_4Ln^{III}_2\}$ (Ln = Dy, Tb) Complexes: Syntheses, Structures, and Magnetic Properties. *Eur. J. Inorg. Chem.* **2015**, 156−165.
(34) Goura, J.; Brambleby, J.; Goddard, P.; Chandrasekhar, V. A Single-Ion Magnet Based on a Heterometallic $Co^{III}_2Dy^{III}$ Complex. *Chem.—Eur. J.* **2015**, *21*, 4926−4930.
(35) Goura, J.; Brambleby, J.; Topping, C. V.; Goddard, P. A.; Narayanan, R. S.; Bar, A. K.; Chandrasekhar, V. Heterometallic Trinuclear $\{Co^{III}_2Ln^{III}\}$ (Ln = Gd, Tb, Ho and Er) Complexes in a Bent Geometry. Field-Induced Single-Ion Magnetic Behavior of the Er^{III} and Tb^{III} Analogues. *Dalton Trans.* **2016**, *45*, 9235−9249.
(36) Liu, K.; Shi, W.; Cheng, P. Toward Heterometallic Single-Molecule Magnets: Synthetic Strategy, Structures and Properties of 3d-4f Discrete Complexes. *Coord. Chem. Rev.* **2015**, *289*−*290*, 74−122.
(37) Wu, J.; Zhao, L.; Zhang, L.; Li, X.-L.; Guo, M.; Tang, J. Metallosupramolecular Coordination Complexes: The Design of

DOI: 10.1021/acsomega.8b00292
ACS Omega 2018, 3, 5202−5211

Heterometallic 3d-4f Gridlike Structures. *Inorg. Chem.* **2016**, *55*, 5514−5519.
(38) Piquer, L. R.; Sañudo, E. C. Heterometallic 3d−4f Single-Molecule Magnets. *Dalton Trans.* **2015**, *44*, 8771−8780.
(39) Colacio, E.; Ruiz-Sanchez, J.; White, F. J.; Brechin, E. K. Strategy for the Rational Design of Asymmetric Triply Bridged Dinuclear 3d-4f Single-Molecule Magnets. *Inorg. Chem.* **2011**, *50*, 7268−7273.
(40) Llunell, M.; Casanova, D.; Cirera, J.; Bofill, J. M.; Alemany, P.; Alvarez, S.; Pinsky, M.; Avnir, D. *SHAPE (2.1)*; Universitat de Barcelona: Barcelona, Spain, 2013.
(41) Chilton, N. F.; Anderson, R. P.; Turner, L. D.; Soncini, A.; Murray, K. S. PHI: A powerful new program for the analysis of anisotropic monomeric and exchange-coupled polynuclear d- and f-block complexes. *J. Comput. Chem.* **2013**, *34*, 1164−1175.
(42) (a) Palacios, M. A.; Mota, A. J.; Perea-Buceta, J. E.; White, F. J.; Brechin, E. K.; Colacio, E. Antiferromagnetic versus Ferromagnetic Exchange Interactions in Bis(μ-Ooximate)dinickel(II) Units for a Series of Closely Related Cube Shaped Carboxamideoximate-Bridged Ni_4 Complexes. A Combined Experimental and Theoretical Magneto-Structural Study. *Inorg. Chem.* **2010**, *49*, 10156−10165. (b) Biswas, R.; Giri, S.; Saha, S. K.; Ghosh, A. One Ferromagnetic and Two Antiferromagnetic Dinuclear Nickel(II) Complexes Derived from a Tridentate N, N,O-Donor Schiff Base Ligand: A Density Functional Study of Magnetic Coupling. *Eur. J. Inorg. Chem.* **2012**, 2916−1927. (c) Nanda, K. K.; Thompson, L. K.; Bridson, J. N.; Nag, K. Linear dependence of spin exchange coupling constant on bridge angle in phenoxy-bridged dinickel(II) complexes. *J. Chem. Soc., Chem. Commun.* **1994**, 1337. (d) Halcrow, M. A.; Sun, J.-S.; Huffman, J. C.; Christou, G. Structural and Magnetic Properties of [Ni4(.mu.3-OMe)4(dbm)-4(MeOH)4] and [Ni4(.eta.1.,mu.3-N3)4(dbm)4(EtOH)4]. Magneto-structural Correlations for [Ni4X4]4+ Cubane Complexes. *Inorg. Chem.* **1995**, *34*, 4167−4177. (e) Clemente-Juan, J. M.; Chansou, B.; Donnadieu, B.; Tuchagues, J.-P. Synthesis, Structure, and Magnetic Properties of the Low-Symmetry Tetranuclear Cubane-like Nickel Complex $[Ni4(pypentO)(pym)(\mu_3\text{-}OH)_2(\mu\text{-}Oac)_2(NCS)_2(OH_2)]$. *Inorg. Chem.* **2000**, *39*, 5515−5519. (f) Bu, X.-H.; Du, M.; Zhang, L.; Liao, D.-Z.; Tang, J.-K.; Zhang, R.-H.; Shionoya, M. Novel nickel(II) complexes with diazamesocyclic ligands functionalized by additional phenol donor pendant(s): synthesis, characterization, crystal structures and magnetic properties. *J. Chem. Soc., Dalton Trans.* **2001**, 593−598.
(43) Singh, S. K.; Tibrewal, N. K.; Rajaraman, G. Density Functional Studies on Dinuclear {NiIIGdIII} and Trinuclear {NiIIGdIIINiII} Complexes: Magnetic Exchange and Magneto-Structural Maps. *Dalton Trans.* **2011**, *40*, 10897−10906.
(44) Colacio, E.; Ruiz, J.; Mota, A. J.; Palacios, M. A.; Cremades, E.; Ruiz, E.; White, F. J.; Brechin, E. K. Family of Carboxylate- and Nitrate-Diphenoxo Triply Bridged Dinuclear NiIILnIII Complexes (Ln = Eu, Gd, Tb, Ho, Er, Y): Synthesis, Experimental and Theoretical Magneto-Structural Studies, and Single-Molecule Magnet Behavior. *Inorg. Chem.* **2012**, *51*, 5857−5868.
(45) Meng, Z.-S.; Guo, F.-S.; Liu, J.-L.; Leng, J.-D.; Tong, M.-L. Heterometallic Cubane-like {M2Ln2} (M = Ni, Zn; Ln =, Gd, Dy) and {Ni2Y2} Aggregates: Synthesis, Structures and Magnetic Properties. *Dalton Trans.* **2012**, *41*, 2320−2329.
(46) (a) Roy, L. E.; Hughbanks, T. Magnetic Coupling in Dinuclear Gd Complexes. *J. Am. Chem. Soc.* **2006**, *128*, 568−575. (b) Cañadillas-Delgado, L.; Fabelo, O.; Pasán, J.; Delgado, F. S.; Lloret, F.; Julve, M.; Ruiz-Pérez, C. Intramolecular Ferro- and Antiferromagnetic Interactions in Oxo-Carboxylate Bridged Digadolinium(III) Complexes. *Dalton Trans.* **2010**, *39*, 7286−7293. (c) Cañadillas-Delgado, L.; Fabelo, O.; Cano, J.; Pasán, J.; Delgado, F. S.; Lloret, F.; Julve, M.; Ruiz-Pérez, C. Dinuclear and Two- and Three-Dimensional gadolinium(III) Complexes with Mono- and Dicarboxylate Ligands: Synthesis, Structure and Magnetic Properties. *CrystEngComm* **2009**, *11*, 2131−2142.
(47) (a) Shi, P.-F.; Cao, C.-S.; Wang, C.-M.; Zhao, B. Several [Gd-M] Heterometal−Organic Frameworks with [Gdn] as Nodes: Tunable Structures and Magnetocaloric Effect. *Inorg. Chem.* **2017**, *56*, 9169−9176. (b) Hosoi, A.; Yukawa, Y.; Igarashi, S.; Teat, S. J.; Roubeau, O.; Evangelisti, M.; Cremades, E.; Ruiz, E.; Barrios, L. A.; Aromí, G. A Molecular Pair of [GdNi3] Tetrahedra Bridged by Water Molecules. *Chem.—Eur. J.* **2011**, *17*, 8264−8268. (c) Zheng, Y.-Z.; Evangelisti, M.; Winpenny, R. E. P. Large Magnetocaloric Effect in a Wells-Dawson Type {Ni6Gd 6P6} Cage. *Angew. Chem., Int. Ed.* **2011**, *50*, 3692−3695. (d) Peng, J.-B.; Zhang, Q.-C.; Kong, X.-J.; Ren, Y.-P.; Long, L.-S.; Huang, R.-B.; Zheng, L.-S.; Zheng, Z. A 48-Metal Cluster Exhibiting a Large Magnetocaloric Effect. *Angew. Chem., Int. Ed.* **2011**, *50*, 10649−10652; *Angew. Chem.* **2011**, *123*, 10837. (e) Wang, P.; Shannigrahi, S.; Yakovlev, N. L.; Hor, T. S. A. Facile Self-Assembly of Intermetallic [Ni2Gd2] Cubane Aggregate for Magnetic Refrigeration. *Chem.—Asian J.* **2013**, *8*, 2943−2946. (f) Pasatoiu, T. D.; Ghirri, A.; Madalan, A. M.; Affronte, M.; Andruh, M. Octanuclear [Ni(II)4Ln-(III)4] Complexes: Synthesis, Crystal Structures and Magnetocaloric Properties. *Dalton Trans.* **2014**, *43*, 9136−9142. (g) Hooper, T. N.; Schnack, J.; Piligkos, S.; Evangelisti, M.; Brechin, E. K. The Importance of Being Exchanged: [GdIII4MII8(OH)8(L)8(O2CR)8]4+ Clusters for Magnetic Refrigeration. *Angew. Chem., Int. Ed.* **2012**, *51*, 4633−4636. (h) Das, S.; Dey, A.; Kundu, S.; Biswas, S.; Mota, A. J.; Colacio, E.; Chandrasekhar, V. Linear {NiII−LnIII−NiII} Complexes Containing Twisted Planar Ni(μ-phenolate)2Ln Fragments: Synthesis, Structure, and Magnetothermal Properties. *Chem.—Asian J.* **2014**, *9*, 1876−1887.
(48) (a) Ruiz, J.; Mota, A. J.; Rodríguez-Diéguez, A.; Titos, S.; Herrera, J. M.; Ruiz, E.; Cremades, E.; Costes, J. P.; Colacio, E. Field and Dilution Effects on the Slow Relaxation of a Luminescent DyO9 Low-Symmetry Single-Ion Magnet. *Chem. Commun.* **2012**, *48*, 7916−7918. (b) Bi, Y.; Guo, Y.-N.; Zhao, L.; Guo, Y.; Lin, S.-Y.; Jiang, S.-D.; Tang, J.; Wang, B.-W.; Gao, S. Capping Ligand Perturbed Slow Magnetic Relaxation in Dysprosium Single-Ion Magnets. *Chem.—Eur. J.* **2011**, *17*, 12476−12481. (c) Feltham, H. L. C.; Lan, Y.; Klöwer, F.; Ungur, L.; Chibotaru, L. F.; Powell, A. K.; Brooker, S. A Non-Sandwiched Macrocyclic Monolanthanide Single-Molecule Magnet: The Key Role of Axiality. *Chem.—Eur. J.* **2011**, *17*, 4362−4365 and references therein.
(49) Armarego, W. L. E.; Chai, C. L. L. Purification of Organic Chemicals. *Purification of Laboratory Chemicals*, 5th Ed.; Butterworth-Heinemann An imprint of Elsevier Science: USA, 2003; pp 80−388.
(50) Furniss, B. S.; Hannaford, A. J.; Smith, P. W. G.; Tatchell, A. R. *Vogel's Textbook of Practical Organic Chemistry*, 5th Ed.; Longman group UK Limited: London, 1989; pp 395−469.
(51) You, Z.-L.; Shi, D.-H.; Zhang, J.-C.; Ma, Y.-P.; Wang, C.; Li, K. Synthesis, Structures, and Urease Inhibitory Activities of oxovanadium(V) Complexes with Schiff Bases. *Inorg. Chim. Acta* **2012**, *384*, 54−61.
(52) Wang, F.-M. Di-μ-Oxido-bis[(2-Ethoxy-6-{[2-(2-Hydroxyethylamino)ethylimino]methyl}phenolato-κ^3N,N′,O^1)-oxidovanadium(V)]. *Acta Crystallogr., Sect. E: Struct. Rep. Online* **2012**, *68*, m26−m27.
(53) *SMART & SAINT Software Reference manuals*, version 6.45; Bruker Analytical X-ray Systems, Inc.: Madison, WI, 2003.
(54) Sheldrick, G. M. *SADABS, Program for Empirical Absorption Correction*; University of Gottingen: Germany, 1996.
(55) *Bruker APEX2*, version 2008.1−0; Bruker AXS Inc.: Madison, Wisconsin, USA, 2008.
(56) Sheldrick, G. M. SHELXT-Integrated Space-Group and Crystal-Structure Determination. *Acta Crystallogr., Sect. A: Found. Adv.* **2015**, *71*, 3−8.
(57) Sheldrick, G. M. Crystal Structure Refinement with SHELXL. *Acta Crystallogr., Sect. C: Struct. Chem.* **2015**, *71*, 3−8.
(58) Dolomanov, O. V.; Bourhis, L. J.; Gildea, R. J.; Howard, J. A. K.; Puschmann, H. OLEX2: A Complete Structure Solution, Refinement and Analysis Program. *J. Appl. Crystallogr.* **2009**, *42*, 339−341.
(59) Spek, A. L. PLATON SQUEEZE: A Tool for the Calculation of the Disordered Solvent Contribution to the Calculated Structure Factors. *Acta Crystallogr., Sect. C: Struct. Chem.* **2015**, *71*, 9−18.
(60) Brandenburg, K.; Putz, H. *DIAMOND*, version 3.2; Crystal Impact GbR: Bonn, Germany, 1997−2014.

DOI: 10.1021/acsomega.8b00292
ACS Omega 2018, 3, 5202−5211